Launch in orbit of the telescope NINA for cosmic ray observations: preliminary results

R. Sparvoli[a*], V. Bidoli[a], A. Canestro[a], M. Casolino[a], M. P. De Pascale[a], G. Furano[a], A. Iannucci[a], A. Morselli[a], P. Picozza[a], A. Bakaldin[b], A. Galper[b], S. Koldashov[b], M. Korotkov[b], A. Leonov[b], V. Mikhailov[b], A. Murashov[b], S. Voronov[b], V. Bonvicini[c], R. Cirami[c], A. Vacchi[c], N. Zampa[c], M. Ambriola[d], R. Bellotti[d], F. Cafagna[d], F. Ciacio[d], M. Circella[d], C. De Marzo[d], S. Bartalucci[e], M. Ricci[e], O. Adriani[f], P. Papini[f], S. Piccardi[f], P. Spillantini[f], M. Boezio[g], G. Castellini[h]

[a]Univ. of Rome "Tor Vergata" and INFN section of Roma2, Italy

[b]Moscow Engineering Physics Institute, Moscow, Russia

[c]Univ. of Trieste and INFN section of Trieste, Italy

[d]Univ. of Bari and INFN section of Bari, Italy

[e]INFN Laboratori Nazionali di Frascati, Italy

[f]Univ. of Florence and INFN section of Florence, Italy

[g]Royal Institute of Technology, Stockholm, Sweden

[h]Istituto di Ricerca Onde Elettromagnetiche CNR, Firenze, Italy

On July the 10^{th}, 1998 the telescope NINA was launched in space on board the Russian satellite Resurs-01 n.4. The scientific task of the mission is the study of the galactic, solar and anomalous components of the cosmic rays in the energy interval 10-200 MeV/n for contained particles. The core of NINA is a segmented silicon detector mounted onto the satellite so to point to the zenith.

In this paper we report about the cosmic ray measurements performed by the telescope during its first 6 months of operation.

1. INTRODUCTION

The mission NINA has been conceived by the Italian National Institute of Nuclear Physics (INFN) and the Moscow Engineering and Physics Institute (MEPhI). The INFN representative involves several Italian Institutes and Universities (WIZARD Collaboration) which, together with European and American partners, have carried out balloon-borne experiments since 1989.

The link to the Russian counterpart happened in 1994, when the two sides established a collaboration and conceived the Russian-Italian Missions (RIM), of which NINA (a New Instrument for Nuclear Analysis) is the first step.

NINA's goal is to detect cosmic ray nuclei of galactic, solar or anomalous origin, from hydrogen to iron, between 10 and 200 MeV/n in regime of full containment, and till a few GeV/n when the particles cross the detector [1,2]. The experiment is carried out on board the satellite Resurs-01 n.4, developed by the Russian Space Company VNIIEM, launched on a polar sun-synchronous orbit at 840 km of altitude.

NINA will be soon joint by a twin detector (NINA-2 [3]), that will be placed again on a polar orbit but at a lower altitude (450 km), on board the Italian satellite MITA. The launch is foreseen for December 1999; the presence of this couple

*Dept. of Physics, Univ. of Rome "Tor Vergata" and INFN - Via della Ricerca Scientifica 1, 00133 Rome, Italy. Email: Sparvoli@roma2.infn.it

of detectors will allow estimations of cosmic ray fluxes in different periods of the solar cycle.

2. THE INSTRUMENT NINA

NINA is divided in the following 4 subsystems: the *detector (Box D1)*, composed of 32 silicon layers and the electronics for signal processing, the *on-board computer (Box D2)*, a dual microprocessor dedicated to data processing and to the selection of the trigger and the acquisition mode configuration, the *interface computer (Box E)*, which rearranges the data coming from $D2$ and delivers them to the satellite telemetry system, and the *power supply (Box P)*, which distributes the power supply to the different subsystems. The weight and electric power of the complete telescope are respectively 40 kg and 40 W, in accordance with the constraints imposed by the satellite.

The active part of NINA is a modular telescope composed of 16 planes; every plane consists of two n-type silicon detectors, 60×60 mm^2, each divided in 16 strips orthogonal mounted (X and Y views), thus resulting in a total of 32 silicon detector layers. The thickness of the first pair is 150 μm; all the others, instead, are 380 μm thick, for a total thickness of 11.7 mm of silicon.

Table 1
Energy windows (in MeV/n) for the most abundant particles in NINA detector, in High Threshold configuration

Particle	Z	Energy window
^{1}H	1	10 - 14
^{4}He	2	9 - 47
^{7}Li	3	11 - 54
^{9}Be	4	13 - 65
^{11}B	5	15 - 75
^{12}C	6	17 - 87
^{14}N	7	18 - 95
^{16}O	8	20 - 103
^{19}F	9	21 - 107
^{20}Ne	10	23 - 117
^{28}Si	14	28 - 142
^{40}Ca	20	39 - 175
^{56}Fe	26	58 - 195

The distance between planes is 1.4 cm, except for the first and second which are separated by 8.5 cm, for a better measurement of the particle incident angle. Below the 16 active modules, other 4 cards are placed, dedicated to the trigger electronics, silicon power supply, analog-digital conversion, FIFO. The whole structure is surrounded by a cylindrical aluminum vessel filled up with nitrogen at 1.2 atm.

A system of anticoincidences (AC) acts so to ensure the complete containment of the particle inside the detector, condition allowing the best energy and nuclear discrimination in NINA: the Lateral Anticoincidence is realized with the strips 1 and 16 of every silicon layer, while the Bottom Anticoincidence makes use of the whole plane 16, X and Y view, in order to reject escaping or albedo particles.

The main trigger of the acquisition system is the following:

$$TRG\,M1 = D_{1x} \times D_{1y} \times ((D_{2x} + D_{2y}) + (D_{3x} + D_{3y}))\ ,$$

where D_{ij} is the above-threshold signal coming from the plane i, view j (j=x,y). The logic OR of planes 2 and 3 provides redundancy in case of a failure of plane 2. In the default operating mode, this trigger is used together with the Lateral and Bottom Anticoincidence ON.

It is possible to switch, via telecommand, to a second trigger:

$$TRG\,M2 = (D_{2x} + D_{2y}) \times (D_{3x} + D_{3y}) \times (D_{4x} + D_{4y}) \times (D_{5x} + D_{5y})\ ,$$

which is used again in its basic operating mode with the Lateral and Bottom AC ON. This trigger, used for particular data taking demands or in case of failure of the first plane, increases the acceptance angle, although with a worsening of the angular resolution.

NINA can work in two acquisition modes, which focus two different energy intervals for particles; a so called *Low Threshold mode* favors the acquisition of Z=1 particles, while the *High Threshold mode* is the preferred one for the observation of heavier nuclei.

The acceptance window of particles with TRG M1 and request of full containment of the event

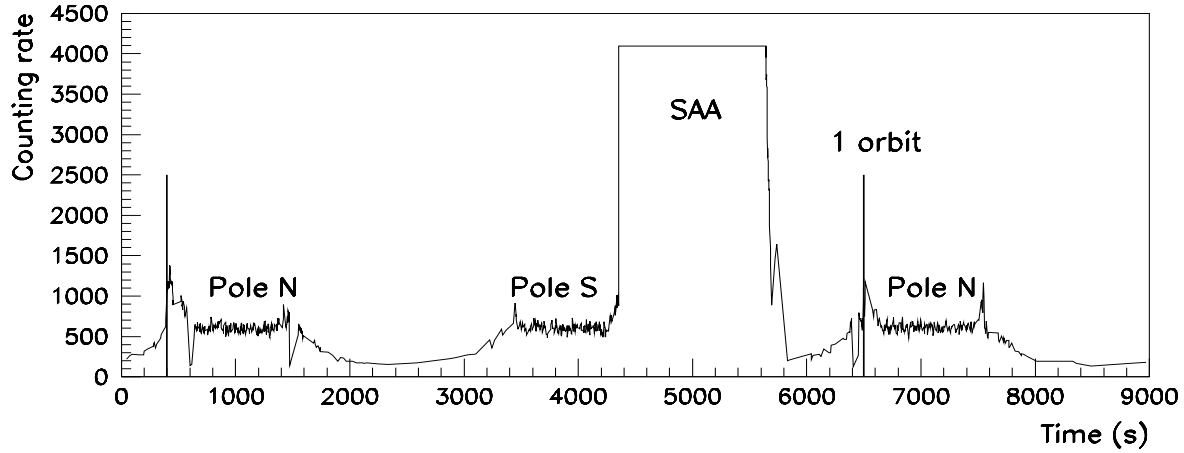

Figure 1. Behavior of NINA counting rate (expressed in ADC channels) as a function of time (seconds); the two black vertical lines define 1 satellite orbit.

is shown in Table 1, for High Threshold. The spectrum of nuclei extends from hydrogen to iron in the energy interval 10 - 200 MeV/n but if the Bottom Anticoincidence is removed, NINA can register nuclei up to a few GeV/n, still with a good nuclear discrimination.

3. DATA ANALYSIS

The optimal performances of NINA in terms of charge, mass and energy determination are achieved by requesting the full containment of the particle inside the detector, ensured by the anticoincidence system. Moreover, a selection algorithm which saves only *good-tagged* events has been implemented. This selection rejects upward moving particles, tracks accompanied by nuclear interactions, and also events consisting of two and more tracks. Moreover, to refrain particles from leaving the detector through the lateral gaps between the planes, the algorithm rejects also events having an energy deposit in lateral strips 2 or 15 for all planes but the first.

The mass M and the charge Z are calculated in parallel by two methods, in order to have a more precise particle recognition:
(a) the method of the residual range [2,4–6];
(b) the method of the approximation to the Bethe-Bloch theoretical curve. This second method finds the mass M and charge Z which minimize the square difference between the real energy deposits of the particle in each silicon detector and the theoretical ones. In order to achieve that, it is necessary to follow step by step the track structure, calculating the scattering angles at every sensitive layer. This method takes into account also the energy losses in the *dead* layers, therefore allows to avoid systematic shifts in the reconstructed masses.

For a rigid rejection of the background, only particles with the same final identification given by the two methods are taken. Finally, a cross-check between the real range of the particle in the detector and its expected one (by simulations) gives the definitive consistence test for the event.

The initial energy of the particle is recovered by summing up the total energy deposited in the whole detector and the restored energy lost in the (dead) aluminum entrance window. This last value is calculated by means of the Bethe-Bloch formula assuming as parameters for the particle the reconstructed mass M, charge Z, and incident angle.

In order to estimate the cosmic ray differential energy spectra it is necessary to know the geometric factor of NINA as a function of the energy, the efficiency of the track selection algorithm, again as a function of the energy, and the exposure time

in orbit. The geometric factor of the instrument, as well as the efficiency of the selection algorithm, are calculated by means of Monte Carlo simulations using the CERN-GEANT code. The exposure time is estimated considering the time of observation of the detector, the loss of time in the data transfer to ground, and the dead time of the instrument.

Figure 1 presents the typical behavior of the counting rate measured by the detector as a function of time; the two vertical black lines define one orbit. The different regions of the Earth's magnetosphere are clearly recognized by the variations of the particle rate: the polar caps, the equatorial regions, and the very intense South Atlantic Anomaly (SAA), where the flux of trapped particles reaches enormously high values, are uniquely identified.

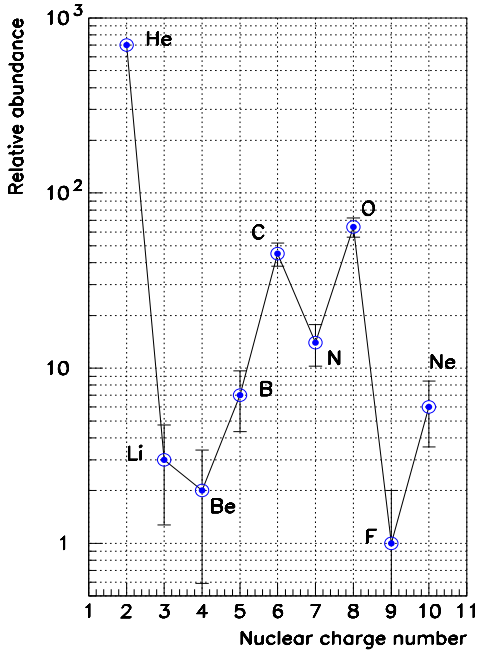

Figure 2. Relative abundance for GCR particles detected by NINA in the solar quiet period December 1998-March 1999.

4. LOW ENERGY COSMIC RAY MEASUREMENTS

The analysis presented in this section refers to particles registered by NINA in the solar quiet period December 1998-March 1999, detected in High Threshold mode and TRG M1 acquisition. In order to select a sample of pure low energy (E>10 MeV/n) primary cosmic rays, and avoid the distortions induced by the Earth magnetic field, only particles registered at a value of L-shell>6 (L geomagnetic shell) have been chosen.

Figure 2 presents the relative abundance for heavy particles as detected by NINA from December 1998 to March 1999. This is a sample of pure galactic cosmic rays, because the filter applied to the data (number of silicon layers crossed>6) excluded the less energetic solar cosmic particles and the anomalous nuclei. The counting rates shown in figure 2 reproduce the existing cosmic ray abundance [7], with the well known odd-even effect, the peaks at carbon and oxygen, and the relative depression of the light elements Li, Be and B.

In figures 3 and 4 we present the differential energy spectra of, respectively, helium between 10 and 50 MeV/n, and carbon and oxygen (together) in the interval 20-100 MeV/n. The helium spectrum (figure 3) below 20 MeV/n can present considerable variations over the months; we present here the average value for the period December 1998-March 1999. The spectra of helium, carbon and oxygen are consistent with previous observations; the apparent absence of a low energy bump in the oxygen spectrum (figure 4) seems to indicate a possible drop of the intensity of the anomalous component at the fall of 1998-beginning of 1999; this might be due to the increase of the solar activity for the 23^{rd} solar cycle.

5. DETECTION OF SOLAR FLARES

Detection of solar energetic particles by NINA occurred mainly in November 1998. Four solar flares were registered in this month, but we report in this section only about two of them: the one of 6^{th}-8^{th} November, where there was a significant increase in the detection of ^{3}He nuclei,

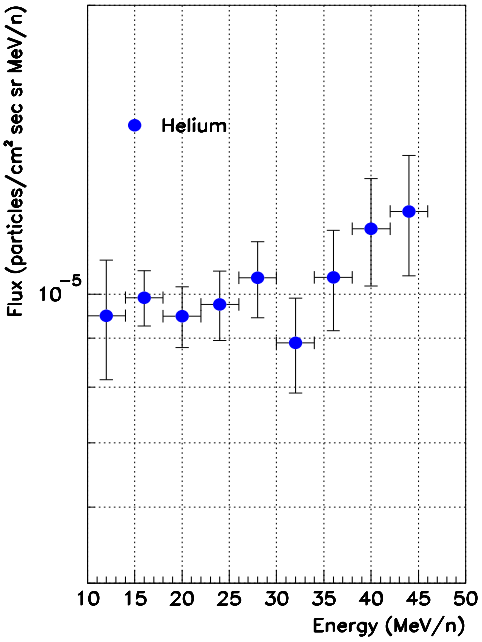

Figure 3. Differential energy spectra for helium in the solar quiet period December 1998-March 1999 as detected by NINA.

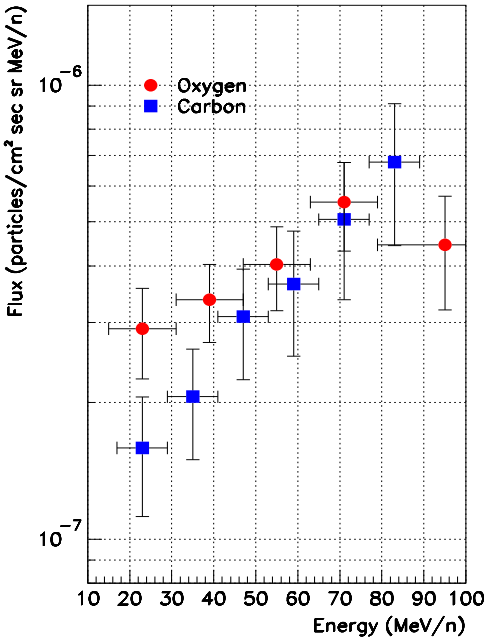

Figure 4. Differential energy spectra for oxygen and carbon in the solar quiet period December 1998-March 1999 as detected by NINA.

and the one of 14^{th}-19^{th} November, during which the nuclear abundance of particles with Z≥2 increased over typical values. Also for flares data the cut L-shell>6 was applied.

During the 6^{th} November flare, a strong increase in the counting rate of Z=1 and Z=2 particles was observed, while no significant acquisition of heavy nuclei was registered. In figure 5 the $dE/dx\,vs\,E$ ($E_1\,vs\,E_{tot}$ for NINA) diagram for helium nuclei during the flare is shown; E_1 is the energy released by the particles in the first silicon plane (two layers) of the detector, and E_{tot} is the total energy released in the whole instrument. By this figure the ^{3}He and ^{4}He nuclei are clearly identified.

The counting rate ratio ^{3}He/^{4}He varied during the flare; the maximum value was reached on November 7^{th} and it was equal to 0.23±0.04.

The differential energy spectra for ^{3}He and ^{4}He in the interval 10-50 MeV/n have been calculated and fitted with a power law function $E^{-\gamma}$. The spectral indexes γ extracted are respectively equal to $\gamma = 2.0\pm0.2$ for ^{3}He and $\gamma = 4.2\pm0.2$ for ^{4}He. The differences in the slopes of the spectra imply an energy dependent ^{3}He/^{4}He ratio; a similar behavior of helium spectra measured in solar flares was observed in early measurements on IMP-5 in the energy interval E ∼ 10-100 MeV/n [8] and on CRRES for the interval E ∼ 50-110 MeV/n [9].

The ratio ^{3}He/^{4}He in these measurements, however, did not exceed a few percents. In the flare of the 6^{th} November 1998, instead, the intensities of ^{3}He and ^{4}He are practically comparable at E ∼ 40 MeV/n. The ratio ^{3}He/^{4}He exceeds of almost one order of magnitude the one observed on the IMP-5 and CRRES satellites at the same energy.

On November the 14^{th} a second strong solar event was observed. This flare differed from the previous one for its enrichment in heavy ions. In figure 6 the diagram $E_1\,vs\,E_{tot}$ for Z≥6 nuclei de-

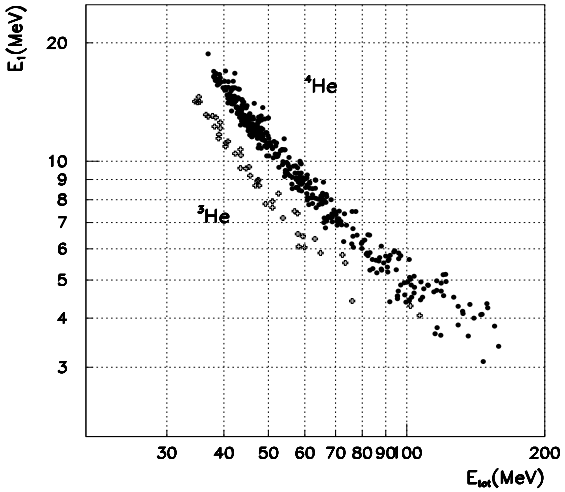

Figure 5. E_1 *vs* E_{tot} diagram for Z=2 particles from the 6^{th} November 1998 flare, as detected by NINA.

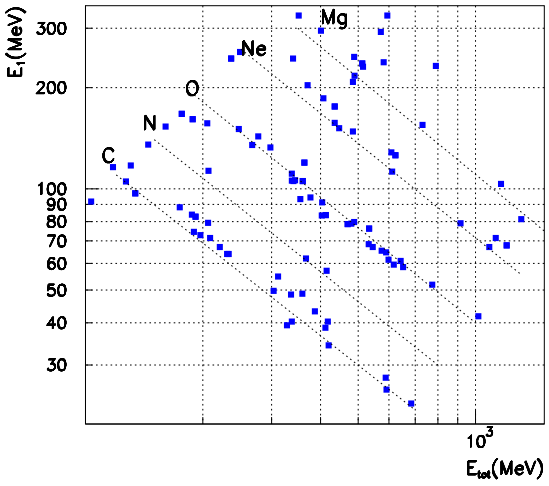

Figure 6. E_1 *vs* E_{tot} diagram for Z$\geq$6 particles from the 14^{th} November 1998 flare, as detected by NINA.

tected in this flare is presented; the relative acquisition of heavy particles in the few hours of the flare compared to the one in quiet time periods was enormously high. The picture shows a qualitative conformity of the flare elemental composition to the one of the solar corona; quantitative nuclear analysis is in progress.

During this flare, finally, no significant acquisition of ^{3}He was registered.

Solar flares were detected by NINA also in January 99; the analysis of such events is in progress.

6. CONCLUSIONS

We presented a preliminary analysis of low energy cosmic rays from hydrogen to neon measured by NINA in solar quiet days (December 1998-March 1999) at L-shell>6, and of solar flares detected by the same instrument in November 1998.

The first look to the data confirmed the good capabilities of the instrument at recognizing particles together with their kinetic initial energy. The comparison of NINA relative abundance's and energy spectra with previous observations is satisfactory. The technical characteristics of the apparatus enables it to detect suddenly increasing fluxes as are the ones produced in solar flares.

A deeper analysis of all the data collected by NINA so far is actually in progress [10,11].

REFERENCES

1. A. Bakaldin et al., Astrop. Phys. 8 109 (1997).
2. V. Bidoli et al., NIM A 424 414 (1999).
3. M. Casolino et al., Proc. 26^{th} ICRC (Salt Lake City) OG 4.2.17 (1999).
4. F. S. Goulding, NIM 162 609 (1979).
5. N. Hasebe et al., NIM A 325 335 (1993).
6. R. Sparvoli et al., Proc. 25^{th} ICRC (Durban), SH 4.5.3 (1997).
7. J. Simpson, Ann. Rev. A&A 33 323 (1983).
8. W. F. Dietrich, ApJ 180 955 (1973).
9. J. Chen et al., ApJ 442 875 (1995).
10. R. Sparvoli et al., Proc. 26^{th} ICRC (Salt Lake City) SH 3.5.01 (1999).
11. M. Casolino et al., Proc. 26^{th} ICRC (Salt Lake City) SH 1.4.04 (1999).